Journal of
Surfaces and Interfaces of Materials
Vol. 2, 252–260, 2014

RESEARCH ARTICLE

Quasi-Solid State Dye-Sensitized Solar Cells with Photoanodes Prepared by Different TiO_2 Precursors Using Sol–Gel Method

D. Sygkridou[1,2], A. Rapsomanikis[1], and E. Stathatos[1,*]

[1] Department of Electrical Engineering, Technological-Educational Institute of Western Greece, Patras, GR-26334, Greece
[2] Physics Department, University of Patras, Patras, 26500, Greece

Thin transparent TiO_2 films, prepared using four different titania precursors (Titanium(IV) isopropoxide, Titanium(IV) butoxide, Titanium(IV) (triethanolaminato) and Diisopropoxytitanium bis(acetylacetonate) have been synthesized by the sol–gel method, keeping the titanium molar ratio constant to all solutions. The films were deposited on conductive glasses using a spin coating device to ensure the films' uniformity and their reproducibility. The structural properties of the TiO_2 films were investigated with scanning electron microscopy (surface and cross section of the films) and porosimetry analysis. The experimental results indicate that the thickness of all the films fabricated with the titanium precursors tested was between 1.5–2 μm. Additionally, these films were used to fabricate dye-sensitized solar cells (DSSCs) to determine if there are any variations to their performance. The results indicated an overall efficiency of 2.94% to the conversion of the solar light to electrical energy measured for cells with photoanodes fabricated with films made from Titanium(IV) butoxide which is 11% higher than that obtained for the widely used Titanium(IV) isopropoxide. Differences to the overall performance were correlated to the structural properties of TiO_2 films and electrical resistances of different interfaces inside the solar cells.

Keywords: TiO_2 Photoanode, Titanium Precursors, Sol–Gel Method, Quasi-Solid State Electrolyte.

1. INTRODUCTION

Over the past decades extensive research has been focused on the development of dye-sensitized solar cells (DSSCs) as a cost effective and environmentally friendly alternative to the conventional amorphous silicon solar cells.[1] Although a variety of wide band gap metal oxides has been tested over the years as photoelectrodes for DSSCs,[2–5] nanocrystalline TiO_2 is the one preferred for the fabrication of highly efficient DSSCs.[6]

The photoanode plays an important role in electron transport and dye adsorption and as a result in the performance of the solar cell, thus, efforts have been made to optimize the photoanode's structural and morphological characteristics.[7–9] Various one-dimensional TiO_2 photoanode nanostructures have been synthesized and examined, such as nanowires,[10,11] nanotubes,[12,13] nanorods,[14,15] nanoflowers,[16] nanoleaves[17] etc. These nanostructures improve the charge collection as the photoinjected electrons are provided with a direct path and they are easily transferred, while in the case of a photoanode with nanoparticles there are numerous defects were electrons can be trapped. However, there are several drawbacks when fabricating a photoanode with one-dimensional TiO_2. The lower surface area results in poor dye loading which eventually affects the short circuit current density and minimizes the overall cell efficiency.

The morphology of the TiO_2 nanoparticles can be affected by the synthesis method applied for the fabrication of the photoanode and the structure of the titanium precursor used. In this work, we investigated four different TiO_2 precursors for optically transparent photoelectrodes synthesized via sol–gel method. Beside the use of Titanium(IV) isopropoxide, which is the most commonly used TiO_2 precursor, we also examined Titanium(IV) butoxide, Titanium(IV) (triethanolaminato) and Diisopropoxytitanium bis(acetylacetonate). The hydrolysis rate minimizes as the isopropoxide groups are substituted by butoxy groups and reduces even more as they are partially replaced by the acetylacetonate groups.[18,19] The photoanodes were used to manufacture DSSCs to establish if

*Author to whom correspondence should be addressed.

2164-7542/2014/2/252/009 doi:10.1166/jsim.2014.1063

there is any effect on their overall energy conversion efficiency and they were also characterized structurally and electrochemically.

2. EXPERIMENTAL DETAILS

2.1. Materials

Commercially available lithium iodide, iodine, 1-methyl-3-propylimidazolium iodide, *tert*-butyl pyridine, guanidine thiocyanate, chloroplatinic acid hexahydrate (H_2PtCl_6), poly(propylene glycol)bis(2-aminopropyl)ether, 3-isocyanatopropyltriethoxysilane and all solvents were purchased from Sigma-Aldrich and used as received. All Titanium precursors, Titanium(IV) isopropoxide (TTIP, 97%), Titanium(IV) butoxide (TTBU, 97%), Titanium(IV) (triethanolaminato) isopropoxide, 80 wt% solution in 2-propanol (TTAI) and Diisopropoxytitanium bis(acetylacetonate) solution (Ti(AcAc)), were also purchased from Sigma-Aldrich (Scheme 1). 3-*Cis*-diisothiocyanato-bis(2,2′-bipyridyl-4,4′-dicarboxylato) ruthenium(II) bis(tetrabutylammonium), N719 was purchased from Solaronix S.A, Switzerland. SnO_2:F transparent conductive electrodes (FTO, TEC8) 8 Ohm/square were purchased from Pilkington NSG Group. Titanium precursors, Triton X-100 (polyethylene glycol *p*-tert-octylphenyl ether) surfactant (99.8%, Fisher Scientific), glacial acetic acid (AcOH, Aldrich) were used to make four different TiO_2 sols.

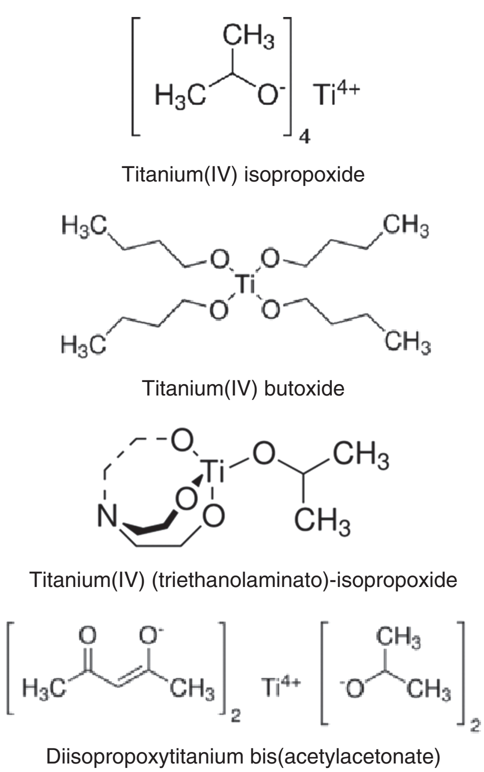

Scheme 1. Molecular structures of the TiO_2 precursors used.

2.2. Preparation of TiO_2 Photoelectrodes

The photoelectrodes were fabricated via sol–gel method using solutions with four different TiO_2 precursors maintaining the same molar ratio.[20,21] Briefly, 0.72 g of Triton X-100 was mixed with 4 ml of ethanol, followed by addition of 0.4 ml of glacial acetic acid and 1.08 mmoles of titanium precursor under vigorous stirring. After a few minutes stirring, the solutions were deposited on the FTO glasses with a spin coating device (Spin150, APT Automation) at 1200 rpm for 10 s. The films were heated up to 500 °C for 30 minutes using 20 °C/min heating ramp rate. The procedure was repeated several times until a satisfactory film thickness was obtained.

2.3. Fabrication and Characterization of Quasi-Solid State Dye-Sensitized Solar Cell

2.3.1. Dye Sensitization of TiO_2 Films

The TiO_2 films prepared by the previously described procedure on FTO glass substrates were immersed into a 0.4 mM (ethanol/acetonitrile 50:50 v/v) solution of N-719 dye and were left there overnight to complete the photoanode sensitization. The glasses were removed from the dye solution and were rinsed with acetonitrile to remove the excessive amount of dye and dried in order to remove any acetonitrile or humidity that could be present in the pores of the films.

2.3.2. Quasi-Solid Electrolyte Preparation

For the fabrication of the solar cells a quasi-solid state electrolyte was used. This was chosen as a promising technique to DSSC technology as it combines the high ionic conductivity of liquids while it reduces the risk of leaks and minimizes sealing problems in the cells. For the gel electrolyte applied to the DSSCs, we used a hybrid organic–inorganic material which was prepared according to a procedure described in previous publications.[22,23] Briefly, poly(propylene glycol)bis(2-aminopropyl ether) of molecular weight 230 and 3-isocyanatopropyltriethoxysilane (ICS; molar ratio ICS/diamine = 2) react in a vessel (acylation reaction), producing urea connecting groups between the polymer units and the inorganic part. The gel electrolyte was synthesized by the following procedure: 0.7 g of the functionalized alkoxide precursor were dissolved in 1.6 g of sulfolane and 0.8 g of 3-methoxypropionitrile under vigorous stirring. Then, 0.368 g AcOH were added followed by 0.12 g LiI, 0.12 g 1-methyl-3-propylimidazolium iodide and 0.06 g I_2. To complete the electrolyte solution, 0.204 g of *tert*-butyl pyridine and 0.036 g of guanidine thiocyanate were added to the above mixture. After six hours stirring, one drop of the obtained sol was placed on the top of the titania electrode with adsorbed dye molecules and a slightly platinized FTO counter electrode was pushed by hand on the top. The platinized FTO glass was made by casting a few drops of H_2PtCl_6 solution (5 mg/1 ml of

Table I. Structural properties of powders obtained from the TiO_2 solutions employing all four precursors.

TiO_2 precursor	Porosity (%)	S_{BET} (m^2/g)	Pore diameter (nm)	Pore volume (cm^3/g)	Pore width (nm)
TTIP	27.14	64.04	4.40	0.098	6.14
TTBU	26.51	60.46	4.45	0.095	6.31
TTAI	26.97	60.33	4.75	0.097	6.48
Ti(AcAc)	27.94	76.08	3.93	0.102	5.40

ethanol) followed by heating at 500 °C for 10 minutes. The two electrodes tightly stuck together by Si–O–Si bonds developed by the presence of the hybrid material.

2.4. Characterization Techniques

The nitrogen sorption/desorption isotherms of all samples were measured with a Micromeritics Tristar 3000 and the surface area, porosity, and pore size distribution were derived by differentiating them according to BET method. All samples were degassed for 2 h at 100 °C before N_2 adsorption analysis. The powders that were used to obtain these values resulted from the titanium solutions. Firstly, the solutions were heated for several hours to 70 °C in order to slowly evaporate the solvent. This resulted to the jellification of the titanium solutions which were afterwards sintered at 500 °C and the obtained agglomerations where grinded to form the powders.

The phase composition of the samples was determined by X-ray diffraction using a Bruker D8 advance diffractometer, with Ni-filtered CuKα radiation ($\lambda = 1.5406$ Å). XRD patterns were obtained from random powder samples in a 2θ range of 2° to 70° at a scanning rate of 2°/min. Random powder mounts of the samples were prepared by gently pressing the powder into the cavity holder.

For the J–V curves, the samples were illuminated with Xe light using a Solar Light Co. solar simulator (model 16S-300) equipped with AM 0 and AM 1.5 direct Air Mass filters to simulate solar radiation at the surface of the earth. The light intensity was kept constant at 1000 W/m^2 measured with a Newport power meter (Model 843-R). Finally, the J–V curves were recorded by connecting the cells to a Keithley Source Meter (model 2601A) which was controlled by Keithley computer software (LabTracer). The cell active area was constant to 0.3 cm^2 using appropriate mask while back reflectors were not used in the measurements. For each case, we made two devices which were tested under the same conditions in order to avoid any misleading estimation of their efficiency. Cell performance parameters, including short-circuit current density (J_{SC}), open circuit voltage (V_{OC}), maximum power (P_{max}), fill factor (FF) and overall cell conversion efficiency, were measured and calculated from each J–V characteristic curve.

Electrochemical impedance spectroscopy measurements (EIS) were carried out under illumination using the same Xe light source that was used for the J–V curves. EIS measurements were performed without the use of a mask with Metrohm Autolab 3 · v potentiostat galvanostat (Model PGSTAT 128N) through a frequency range of 100 kHz–0.01 Hz using a perturbation of ±10 mV over

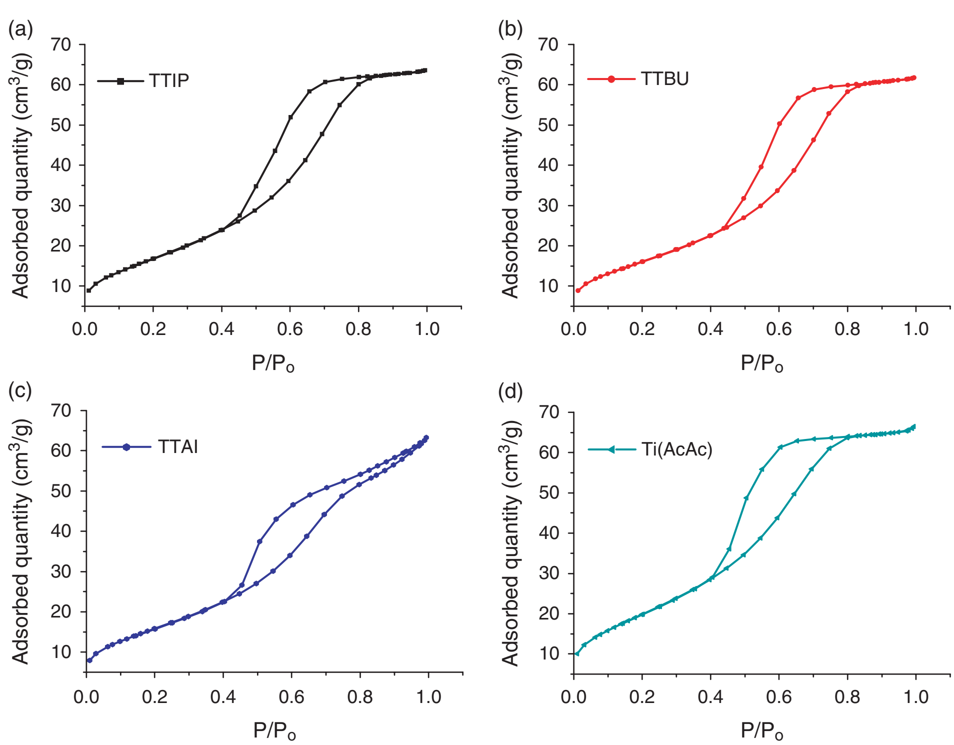

Fig. 1. Sorption–desorption isotherms for powders obtained from the TiO_2 solutions employing (a) TTIP, (b) TTBU, (c) TTAI and (d) Ti(AcAc).

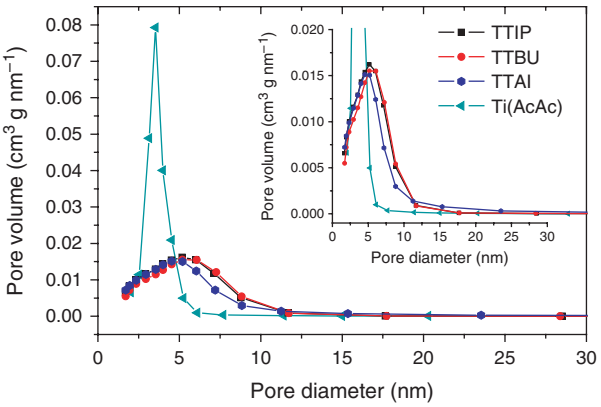

Fig. 2. Pore size distribution for powders obtained from the TiO_2 solutions employing all four precursors.

the open circuit potential. Experimental data are presented by scattering symbols while lines represent the fitted plots obtained using Nova 1.10 software.

3. RESULTS AND DISCUSSION

3.1. Structural Properties of TiO_2 Films

The structural properties of the powders scratched from as prepared films using different titanium oxide precursors, were analyzed with N_2 sorption–desorption. The particle surface area and pore structure of all measured samples are summarized in Table I while the results are presented in Figures 1(a)–(d) and Figure 2.

As it seems in Figure 1 the hysteresis loop appears at low relative pressure ($0.4 < P/P_0 < 0.8$) which is attributed to smaller mesoporosity of the material. The sample's Brunauer, Emmett and Teller (BET) specific surface area was high while the Barrett, Joyner and Halenda (BJH) pore volume (Fig. 2) was relatively low at 0.09–0.1 cm^3/g. Moreover, all the samples obtained from the different TiO_2 precursors had a small mean pore diameter, with the powder resulted from Ti(AcAc) precursor appear the smallest pore diameter among all.

The particle's size was verified through the SEM images of the surface of the films which are presented in Figure 3. The films employing TTIP and TTBU had similar particle size (9–13 nm) while Ti(AcAc) had the smallest particle size (6–9 nm). It is obvious that all films prepared from the four different titanium precursors are consisted of TiO_2 particles of very small in size. In addition, based on SEM cross section images, the films were thin and their thickness was approximately between 1.5–2 μm. Figure 4 shows the cross section of the film prepared from TTBU precursor as an example.

XRD patterns of the powders prepared from different precursors are shown in Figure 5. The diffraction peak at around 25° represents the anatase form of TiO_2 while the peak's intensity observed which is higher for the case of TTBU suggests a larger amount of TiO_2. The grain size for anatase TiO_2 particles has been calculated from XRD patterns using Scherrer's equation: $D = 0.9\ \lambda/(s\cos\theta)$, where λ is the wavelength of the X-ray and s is the full width (radians) at half maximum (FWHM) of the signal.

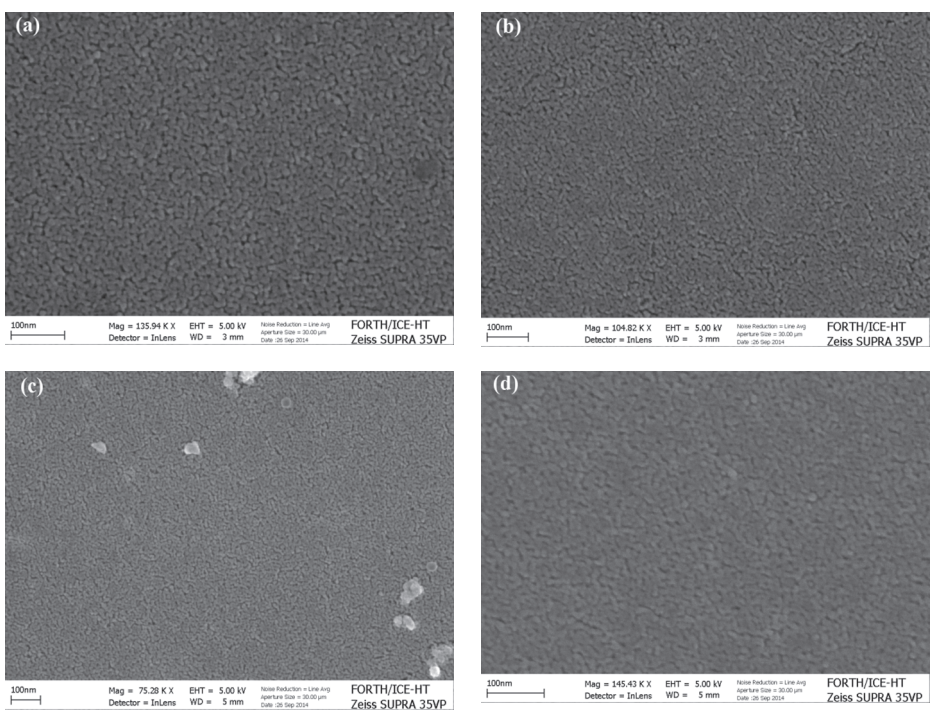

Fig. 3. SEM images of (a) TTIP, (b) TTBU, (c) TTAI and (d) Ti(AcAc).

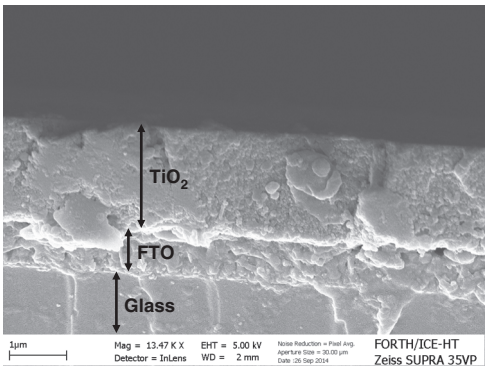

Fig. 4. Cross section of the film employing TTBU.

The crystallite size for TiO_2 prepared from TTIP, TTBU, TTAI, Ti(AcAc) precursors is calculated as 9.5, 12.7, 14.8, 7.3 respectively which is in good accordance to the SEM images. Moreover, the peak at around 27° corresponds to the rutile form of TiO_2. The fact that this peak isn't distinctive for the case of TTAI and Ti(AcAc) might be an explanation why the cells employing those photoanodes performed poorly compared with the cells with TTBU and TTIP as it can be seen to the solar cell performance section.

Figure 6 shows the absorption spectra of the different TiO_2 films. Beside the spectrum corresponding to the film employing TTAI, all the other spectra exhibit interference fringes. Since the TiO_2 molar ratio was kept constant for all starting solutions, the quantity of titanium was the same for all films. Thus, the fact that fringes occur to thicker films, indicates that films which resulted from the solutions containing TTIP, TTBU and Ti(AcAc) were more porous (or less dense). However, the TTAI films weren't uniform throughout the surface which led to poor dye adsorption. Additionally, from the steep part of the spectra at the absorbance threshold wavelength the energy band gap of the TiO_2 was calculated to be 3.4 eV which is in accordance to the values obtained for mesoporous films reported in literature.[24]

3.2. Solar Cells Performance

Figure 7 presents the current density–voltage (J–V) characteristic curves of quasi solid-state dye sensitized solar cells for all the TiO_2 precursors tested. All J–V measurements were carried out using a mask with an aperture area of 0.3 cm^2. The electrical parameters measured and calculated for all cells are summarized in Table II. The cells' open circuit voltage was relatively constant while differences were detected on the short circuit current density measured. The obtained J_{sc} values were sufficiently high, given the fact that the photoanodes' thickness was relatively small and the fact that the cells had high transparency.

It was interesting to note that cells manufactured with photoanodes which resulted from the use of TTBU, showed higher short circuit current density compared with the ones employing the commonly used TTIP. Specifically, the obtained J_{sc} value for the TTBU was almost 9% higher than the one recorded for the TTIP, which resulted in an

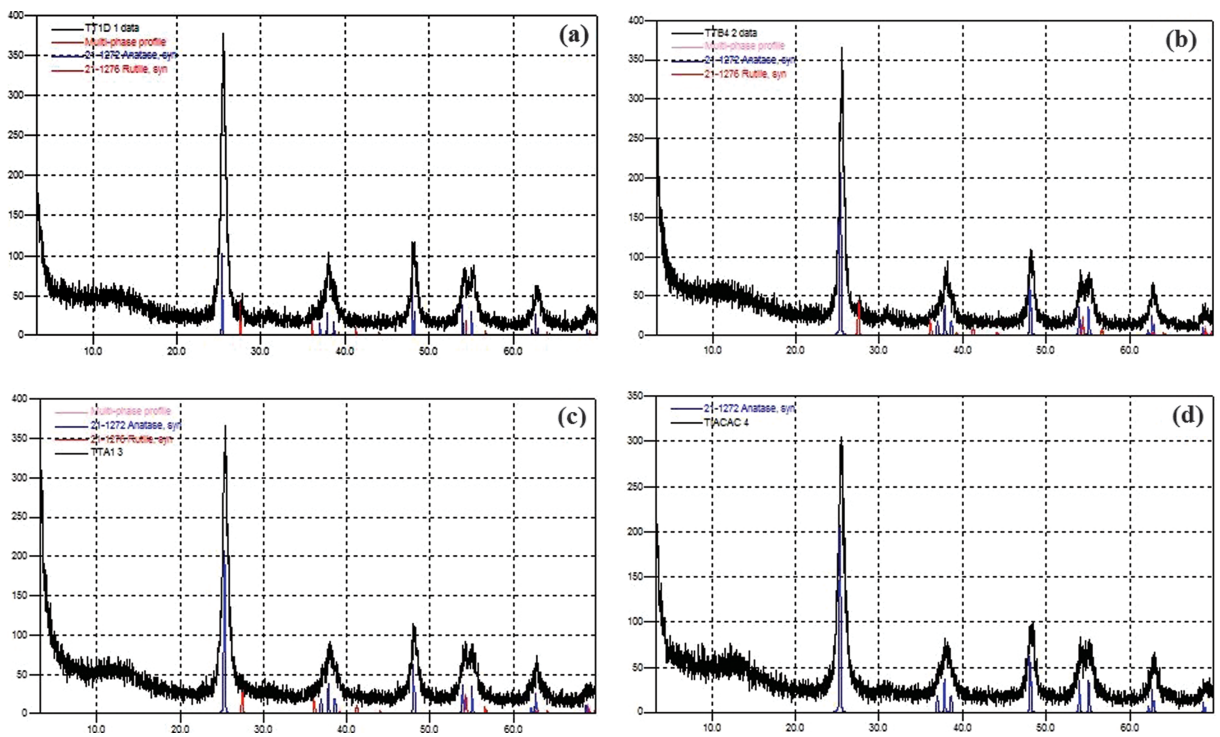

Fig. 5. XRD for powders obtained from the TiO_2 solutions employing (a) TTIP, (b) TTBU, (c) TTAI and (d) Ti(AcAc).

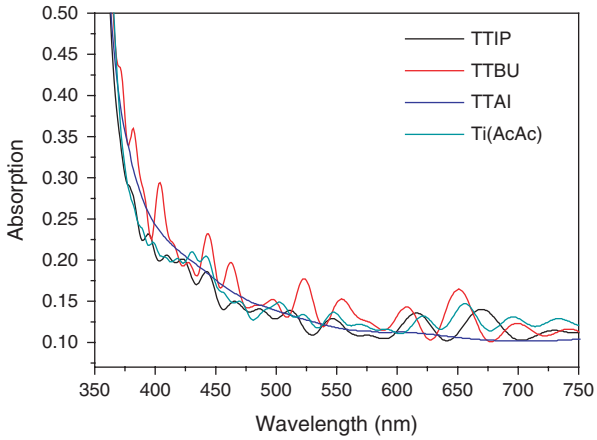

Fig. 6. UV-Vis absorption spectra of TiO_2 films obtained using different precursors.

11.2% increase of the cell's overall efficiency. The photoanodes of the cells prepared with TTAI weren't properly sensitized which justifies the resulting low J_{sc} value.

The dark current suppression was also examined to perceive the extent of the back electron transfer. Figure 8 shows that dark current density in the cells made with the different titanium precursors. The onset of the dark current for the DSSCs fabricated with TTIP, TTBU and Ti(AcAc) occurred at lower voltage compared with TTAI cells, despite the poor dye adsorption of the photoanodes with this alkoxide.

3.3. Electrochemical Impedance Spectroscopy (EIS)

Figures 9(a)–(b) show the Nyquist and Bode plots obtained from cells with the different titanium precursors. The first semicircle corresponds to the Pt/electrolyte interface, R_{pt}. The charge transfer resistance at the counter electrode (R_{pt}) is represented as a semicircle in the impedance spectra and a peak in the Bode phase angle plot. The resistance element related to the response in the intermediate frequency represents the charge transport at the TiO_2/dye/electrolyte interface (R_{tr}) and shows diode like behavior. The semicircle at the low frequency is attributed to the diffusion in the electrolyte (R_{dif}) and the intercept of the horizontal axis stands for the resistance of the sheet resistance of the FTO substrate and the contact resistance of the FTO/TiO_2 (R_h).

Table II. Solar cells parameters for DSSCs with TiO_2 photoelectrodes obtained using different precursors.

TiO_2 precursor	J_{sc} (mA/cm^2)	V_{oc} (Volts)	FF	n (%)
TTIP	6.1	0.692	0.62	2.61
TTBU	6.7	0.693	0.64	2.94
TTAI	1.1	0.694	0.59	0.46
Ti(AcAc)	4.8	0.673	0.65	2.07

The total series resistance of the cell can be calculated using Eq. (1).

$$R_S = R_h + R_{pt} + R_{dif} \quad (1)$$

The equivalent circuits which were used to fit the experimental data are presented in Figure 10. For electrodes having a rough surface the capacitance element in Figure 10(a) is replaced by a constant phase element (CPE, Q) which depends on the parameters Y_o and N. It is possible to convert a CPE element, which is in parallel with a resistance, to a pseudo capacitance using Eq. (2).

$$C_{pseudo} = Y_O^{1/N} \cdot R^{(1/N-1)} \quad (2)$$

The fitted parameters are presented in Table III. The cells whose photoanodes resulted from TTBU had the highest short circuit current density which can be attributed to the fact that they had the smallest total series resistance R_s. As indicated above (Fig. 7), cells with TTIP outperformed the ones with Ti(AcAc), however the total series resistance of the former was higher than the latter. Nevertheless, this inconsistency can be ascribed to the fact that the value of R_h of the cells with Ti(AcAc) was nearly half compared with the one corresponding to the cells with

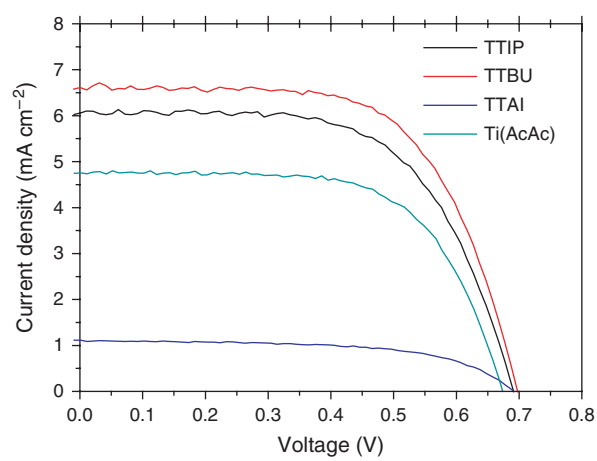

Fig. 7. Photocurrent–voltage curves of DSSCs with photoanodes obtained using different TiO_2 precursors.

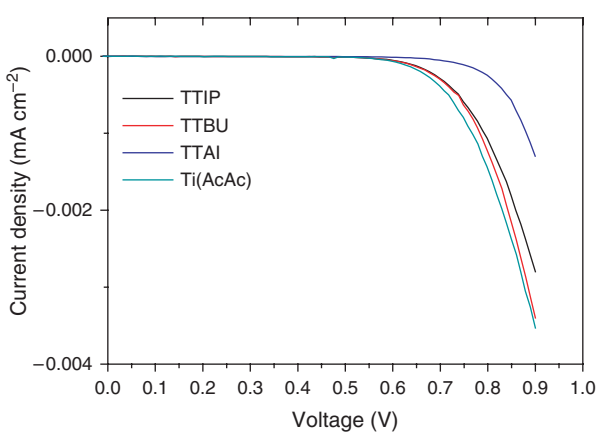

Fig. 8. Dark current–voltage characteristic curves of dye-sensitized solar cells with different TiO_2 precursors.

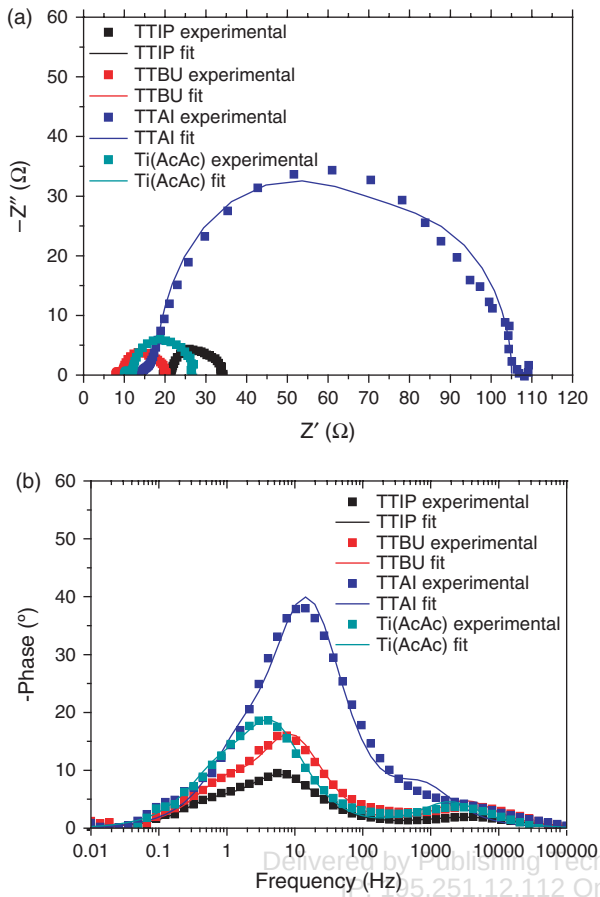

Fig. 9. (a) Impedance spectra and (b) Bode phase plots of dye-sensitized solar cells with different titanium precursors measured at open circuit voltage at 1 sun illumination.

TTIP. Since all the cells were manufactured using the same type of conductive substrate this difference is due to the contact resistance of the FTO/TiO_2. The use of Ti(AcAc) leads to the formation of smaller nanoparticles that are tightly binded on the FTO glasses which results in a small R_h value.

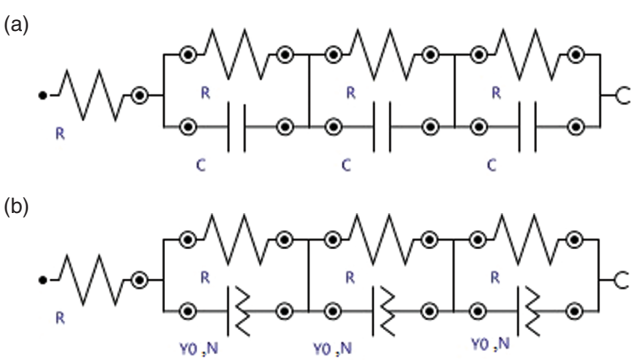

Fig. 10. DSSCs equivalent circuits (a) R(RC)(RC)(RC) and (b) R(RQ)(RQ)(RQ) used to fit the experimental data from the EIS measurements.

Table III. Fitted parameters derived from electrochemical impedance spectroscopy.

Precursor	R_h (Ω)	R_{pt} (Ω)	$C_{pt}*10^{-4}$ (F)	R_{tr} (Ω)	$C_{tr}*10^{-3}$ (F)	R_{dif} (Ω)	$C_{dif}*10^{-2}$ (F)
TTIP	19.50	2.01	0.237	9.10	3.34	3.43	9.32
TTBU	8.07	1.43	0.371	6.56	3.57	3.99	5.35
TTAI	14.40	3.46	0.646	53.20	0.40	34.00	0.39
Ti(AcAc)	10.10	1.73	0.512	8.92	5.14	6.70	3.87

From the peak at the Bode phase plots (Fig. 9(b)) the electron lifetime can be calculated using Eq. (3). The results are summarized in Table IV[25–27]

$$\tau = \frac{1}{2 \cdot \pi \cdot f} \tag{3}$$

Ti(AcAc) had the highest electron lifetime, followed by TTIP and TTBU. These results are not in accordance to the J_{sc} values obtained from J–V curves. However, the small size of TiO_2 particles obtained for films prepared from Ti(AcAc) precursor could prevent the electrons recombination due to better contact of the particles.

The electron lifetime can also be calculated by the open circuit voltage decay (OCVD) technique (Fig. 11(a)) by using Eq. (4)

$$\tau_n = -\frac{k_B \cdot T}{e} \cdot \left(\frac{dV_{OC}}{dt} \right)^{-1} \tag{4}$$

where $(k_B \cdot T)/e = 25.6$ mV where $k_B \cdot T$ is the thermal energy and e is the elementary charge. For this procedure cells are illuminated until they reach a steady open circuit voltage, then the light is interrupted and the charge on the electrodes is allowed to decay in the dark. In this measurement we only included cells with TTIP, TTBU and Ti(AcAc) to compare and determine any differences between them, while the cell with TTAI was excluded as we anticipated a poor representation mainly due to the poor sensitization of the anode.[28] It was observed that the OCVD response of the DSSC consisted of TiO_2 made of TTBU was much slower than that made of TTIP or Ti(AcAc). Electron lifetime (τ_n) was proposed to quantify the extent of electron recombination with the redox electrolyte and has been proven to be effective. Electron lifetime was calculated according to Eq. (4). Figure 11(b) compares the results of the dependence of electron lifetime on the open circuit voltage for DSSCs made of different titanium precursors. It is obvious than in the case of TTBU

Table IV. Electron lifetime derived from the bode phase plots.

Precursor	f (Hz)	τ_n*10^{-2} (s)
TTIP	5.57	2.86
TTBU	7.64	2.09
TTAI	14.24	1.12
Ti(AcAc)	4.04	3.94

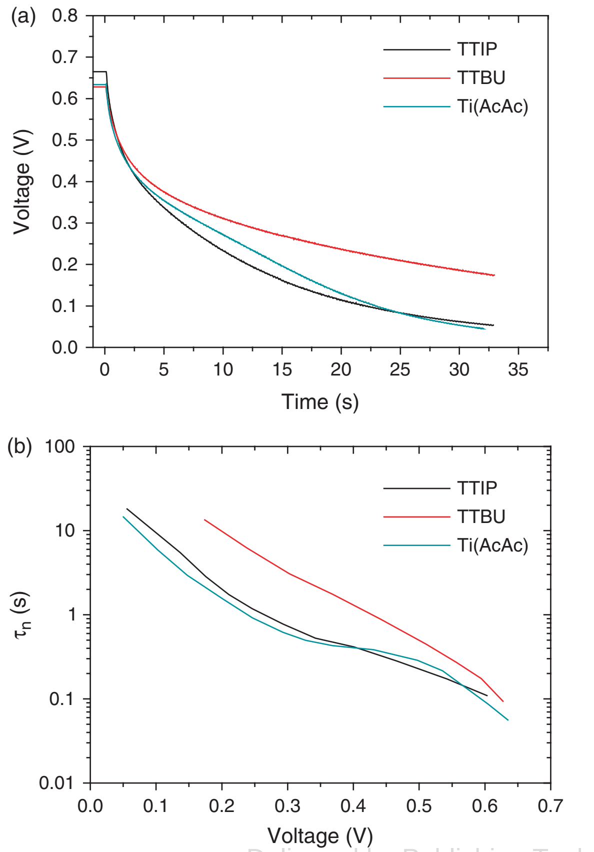

Fig. 11. (a) Open circuit voltage-decay measurement of DSSCs with electrodes obtained with different TiO_2 precursors to illumination excitation (AM 1.5G solar light (100 mWcm^{-2})). (b) Electron lifetime curves in relation to the open circuit voltage for electrodes obtained with different TiO_2 precursors.

electron lifetime was longer than those obtained for the other two precursors. This suggests that electrons injected from excited dye molecules can survive longer without undergoing losses.

4. CONCLUSIONS

TiO_2 photoanodes were prepared by four different TiO_2 precursors using the sol–gel method. The photoanodes' structural properties were tested, as well as the electrical characteristics of the DSSCs assembled employing these electrodes. The photoanodes had almost the same film thickness however, results showed that the cells with TTIP and TTBU performed better than the ones with the TTAI and Ti(AcAc). Particularly, the photoanode which resulted from TTAI wasn't sufficiently sensitized and TTAI along with Ti(AcAc) didn't exhibit any diffraction peaks corresponding to the rutile form of TiO_2 instead of TTIP and TTBU that did. Cells with the TTBU electrode provided the highest electrical parameters and a conversion efficiency of 2.94% which is 11.2% higher that the efficiency of the cell with the widely preferred TTIP, which is also more expensive. The enhanced short circuit current density can be attributed to the fact that the cells with TTBU had smaller internal resistances corresponding to the different interfaces of the cell leading to a smaller total series resistance.

Acknowledgments: This research has been co-financed by the European Union (European Social Fund-ESF) and Greek national funds through the Operational Program "Education and Lifelong Learning" of the National Strategic Reference Framework (NSRF)-Research Funding Program: ARCHIMEDES III, Investing in knowledge society through the European Social Fund. The authors would also like to thank Dr. Vassilios Dracopoulos, FORTH/ICE-HT, for the FE-SEM images and Assistant Professor Dimitrios Papoulis of the University of Patras for the XRD measurements.

RESEARCH ARTICLE

References and Notes

1. A. Hagfeldt, G. Boschloo, L. Sun, L. Kloo, and H. Pettersson, *Chem. Rev.* 110, 6595 (**2010**).
2. M. Zi, M. Zhu, L. Chen, H. Wei, X. Yang, and B. Cao, *Ceram. Int.* 40, 7965 (**2014**).
3. Q. Zhang, C. S. Dandeneau, X. Zhou, and G. Cao, *Adv. Mater.* 21, 4087 (**2009**).
4. A. Birkel, Y.-G. Lee, D. Koll, X. V. Meerbeek, S. Frank, M. J. Choi, Y. S. Kang, K. Char, and W. Tremel, *Energy Environ. Sci.* 5, 5392 (**2012**).
5. R. Ghosh, M. K. Brennaman, T. Uber, M.-R. Ok, E. T. Samulski, L. E. McNeil, T. J. Meyer, and R. Lopez, *ACS Appl. Mater. Interfaces* 3, 3929 (**2011**).
6. B. Hu, Q. Tang, B. He, L. Lin, and H. Chen, *J. Power Sources* 267, 445 (**2014**).
7. A. J. Frank, N. Kopidakis, and J. V. Lagemaat, *Coord. Chem. Rev.* 248, 1165 (**2004**).
8. C.-H. Zhou, S. Xu, Y. Yang, B.-C. Yang, H. Hu, Z.-C. Quan, B. Sebo, B.-L. Chen, Q.-D. Tai, Z.-H. Sun, and X.-Z. Zhao, *Electrochim. Acta* 56, 4308 (**2011**).
9. K. E. Lee, M. A. Gomez, S. Elouatik, and G. P. Demopoulos, *Langmuir* 26, 9575 (**2010**).
10. Z.-J. Zhou, J.-Q. Fan, X. Wang , W.-H. Zhou, Z.-L. Du, and S.-X. Wu, *Appl. Mater. Interfaces* 3, 4349 (**2011**).
11. X. Feng, K. Shankar, O. K. Varghese, M. Paulose, T. J. Latempa, and C. A. Grimes, *Nano Lett.* 8, 3781 (**2008**).
12. D. Wang, B. Yu, F. Zhou, C. Wang, and W. Liu, *Mater. Chem. Phys.* 113, 602 (**2009**).
13. X. Wang, L. Sun, S. Zhang, and X. Wang, *Appl. Mater. Interfaces* 6, 1361 (**2014**).
14. J. Wang, T. Zhang, D. Wang, R. Pan, Q. Wang, and H. Xia, *J. of Alloys and Compounds* 551, 82 (**2013**).
15. S.-M. Wang, W.-W. Dong, R.-H. Tao, Z.-H. Deng, J.-Z. Shao, L.-H. Hu, J. Zhu, and X.-D. Fang, *J. Power Sources* 235, 193 (**2013**).
16. Y. Jiang, M. Li, R. Ding, D. Song, M. Trevor, and Z. Chen, *Mater. Lett.* 107, 210 (**2013**).
17. V. Dhas, S. Muduli, S. Agarkar, A. Rana, B. Hannoyer, R. Banerjee, and S. Ogale, *Solar Energy* 85, 1213 (**2011**).
18. C. J. Barbé, F. Arendse, P. Comte, M. Jirousek, F. Lenzmann, V. Shklover, and M. Grätzel, *J. Am. Ceram. Soc.* 80, 3157 (**1997**).
19. S. Kambe, K. Murakoshi, T. Kitamura, Y. Wada, S. Yanagida, H. Kominami, and Y. Kera, *Sol. Energy Mater. Sol. Cells* 61, 427 (**2000**).

20. E. Stathatos, P. Lianos, A. Surca Vuk, and B. Orel, *Adv. Funct. Mater.* 14, 45 **(2004)**.
21. E. Stathatos, P. Lianos, and C. Tsakiroglou, *Microporous Mesoporous Mater.* 75, 255 **(2004)**.
22. E. Stathatos, *Ionics* 11, 140 **(2005)**.
23. E. Stathatos, P. Lianos, U. L. Stangar, B. Orel, and P. Judeinstein, *Langmuir* 16, 8672 **(2000)**.
24. E. Gondek, P. Karasiński, and S. Drewniak, *Physica E* 62, 128 **(2014)**.
25. J. Bisquert and R. A. Marcus, *Top. Curr. Chem.* 352, 325 **(2013)**.
26. F. Fabregat-Santiago, G. Garcia-Belmonte, I. Mora-Seró, and J. Bisquert, *Phys. Chem. Chem. Phys.* 13, 9083 **(2011)**.
27. M. Pan, N. Huang, X. Zhao, J. Fu, and X. Zhong, *Journal of Nanomaterials* Article 760685 **(2013)**.
28. A. Zaban, M. Greenshtein, and J. Bisquert, *Chem. Phys. Chem.* 4, 859 **(2003)**.

Received: 2 November 2014. Accepted: 8 December 2014.

RESEARCH ARTICLE